

Metabolic Flux Analysis of Embryonic Stem Cells Using Three Distinct Differentiation Protocols and Comparison to Gene Expression Patterns

Darío E. Sepúlveda and Barbara A. Andrews

Institute for Cell Dynamics and Biotechnology: A Centre for Systems Biology, Centre for Biochemical Engineering and Biotechnology, University of Chile, Beauchef 850, Santiago, Chile

Eleftherios Terry Papoutsakis

Dept. of Chemical Engineering, Delaware Biotechnology Institute, University of Delaware, Newark, DE 19716

Juan A. Asenjo

Institute for Cell Dynamics and Biotechnology: A Centre for Systems Biology, Centre for Biochemical Engineering and Biotechnology, University of Chile, Beauchef 861, Santiago, Chile

DOI 10.1002/btpr.448

Published online June 1, 2010 in Wiley Online Library (wileyonlinelibrary.com).

Metabolic flux analysis (MFA) was performed on mouse embryonic stem cells cultured under three distinct differentiation conditions: classical embryoid body formation (EB), and on surfaces coated with either gelatin (GEL) or matrigel (MAT). MFA was based on 15 metabolic reactions and eight transport steps, and was carried out based on measurements of four substrates and/or metabolites: glucose, lactate, glutamine, and glutamate. Fluxes representing biomass production remained fairly constant for all three culture conditions with at most a 40% variation. In contrast, major temporal variations, up to 500%, were observed for all other major central metabolic fluxes across all culture conditions. Fluxes were compared to gene-expression patterns measured by microarray analysis. Particularly interesting is the correlation between the metabolic fluxes with expression patterns of the corresponding genes of the pyruvate to lactate reaction, whereby the genes for several isoforms of the lactate dehydrogenase enzyme were examined. The patterns of this flux were notably different in the EB cultures compared to the GEL and MAT cultures and reflected differences in oxygen and nutrient transport in EB vs. the GEL and MAT cultures. Another novel finding of this study is an event occurring between Days 4 and 5 of differentiation, which was identified by a notable change in both the metabolic fluxes and gene-expression patterns. This suggests that metabolic patterns can be used as effective beacons of changes in differentiating stem cells. Overall, and qualitatively, core metabolic fluxes, under the three culture conditions examined, correlated well with gene-expression patterns. © 2010 American Institute of Chemical Engineers *Biotechnol. Prog.*, 26: 1222–1229, 2010

Keywords: embryonic stem cell, differentiation, MFA, metabolic flux analysis, gene expression profile, lactate, oxidative phosphorylation, hypoxia, embryoid body

Introduction

Embryonic stem (ES) cells are isolated from the embryo epiblast and can be maintained in culture as a cell line.^{1,2} They have the potential to differentiate into any tissue type depending on the culture conditions used, the supporting scaffold, and the scaffold's chemical properties.^{3–6} Several studies have reported differentiation toward lineages, such as cardiac muscle,⁷ neuronal cells,⁸ and pancreatic beta-islet cells,⁹ although tissue-specific cell yields are typically low. Because of their exceptional differentiation potential, ES cells are considered as a potential source of cells for regenerative medicine applications, toxicology studies, and basic

developmental biology. Stem-cell bioengineering plays a crucial role in ultimately realizing the potential of ES cells, and aims to develop the culture conditions and the necessary culture scale needed to achieve desired differentiation outcome, cell yields and purity. Its aim is to identify and acquire the basic biological knowledge needed for achieving these goals.

Metabolic flux analysis (MFA) is a broadly accepted tool for quantifying cellular metabolism and how it varies with culture conditions or in response to stimuli of cellular proliferation and/or differentiation. In the context of cultured cells, MFA has been used to analyze cellular metabolism of CHO¹⁰ and hybridoma cells.¹¹ These studies have been directed to the optimization of culture medium. Other studies involving more complex cells and tissues aim to understand physiological and pathophysiological states associated with important human diseases or tissue engineering applications,

Additional Supporting Information may be found in the online version of this article.

Correspondence concerning this article should be addressed to D. E. Sepúlveda at dsepulveda@ug.uchile.cl.

such as in liver cells^{12,13} or adipocytes.¹⁴ Global-scale microarray-based transcriptional analysis has now been established as an indispensable tool for understanding complex cellular phenotypes, and has experienced an explosive growth over the past 10–12 years. However, relatively few studies have explored possible quantitative or qualitative correlations between gene expression and flux data, either in prokaryotic (e.g.¹⁵) or eukaryotic systems (e.g.¹²). These and other studies so far paint a complex but nevertheless positive picture of what can be gained by parallel gene-expression and flux analysis.

ES-cell development and differentiation remains a complex problem, and in the context of regenerative medicine applications and bioreactor or cell-culture design, the cellular metabolism of differentiating ES cells remains poorly understood. Although many studies on metabolic analysis in mammalian cells have been reported, mainly using mammalian cells as models of human metabolic diseases^{12–14,16} or in industrial cell-culture optimization,^{17,18} to the best of our knowledge, no published work has addressed the metabolic analysis of cellular metabolism of differentiating ES cells. Significantly, there have been no reported studies where flux analysis has been used in conjunction with microarray-based transcriptional analysis to examine the metabolism of differentiating stem cells, whether embryonic or adult.

We have recently examined the impact of culture and differentiation conditions on the gene-expression profile of murine ES cells.¹⁹ Specifically, we used three differentiation protocols and found a decrease in the expression of genes ontologically related to cell metabolism. This raised questions regarding the situation of cell metabolism during differentiation, and it was decided to take a closer look at the metabolism of differentiating cells. In this article the use of a relatively simple reaction network to carry out MFA based on experimental metabolite measurements under the three distinct culture conditions was investigated. Furthermore, we examined the correlation between the estimated fluxes and the microarray genetic-expression profiling in these three differentiation protocols.

Materials and Methods

Chemicals and materials

Nonessential amino acids, sodium pyruvate and fetal calf serum were obtained from Gibco-Invitrogen (Carlsbad, CA), high glucose DMEM, gelatin, penicillin/streptomycin were purchased from Sigma (St. Louis, MO), and Leukemia Inhibitory Factor (LIF) from Chemicon Int. (Temecula, CA). Matrigel matrix (Growth Factor Reduced; MATGFR) was purchased from BD Biosciences (San Diego, CA). The total RNA isolation mini kit, Low RNA input fluorescent linear amplification kit, mouse oligo microarrays (G4121A) and hybridization kits were purchased from Agilent Technologies (Wilmington, DE).

Embryonic-cell cultures

Murine ES R1 cells²⁰ (a gift from Dr. Peter Zandstra, University of Toronto) were cultured as previously described.¹⁹ Briefly, cells were cultured on gelatin-coated flasks in DMEM high glucose, with 0.1 mM nonessential amino acids, 1 mM sodium pyruvate, 100 mM 2-ME, 2 mM L-glutamine, 15% fetal bovine serum, penicillin/streptomycin 50 mg/mL each, and 1000 U LIF/mL, in a humidified incubator at 37°C

with 5% CO₂. For the differentiation protocols, the same medium was used but without sodium pyruvate and LIF. Three conditions were used for cell differentiation: embryoid body formation (EB), where cells were allowed to form three dimensional EB structures, or differentiation on plates coated with gelatin (GEL) or Matrigel (MAT). Cell samples were collected and flash frozen in liquid nitrogen for microarray analysis.

DNA-microarray analysis

DNA microarray analysis was performed as previously described.¹⁹ Raw and normalized data were deposited in the Gene Expression Omnibus (GEO; GSE8574; <http://www.ncbi.nlm.nih.gov/geo/>). Briefly, we used the Agilent microarray technology and a global reference design so that all samples can be compared against any other sample in this study. The common reference RNA was generated by pooling a large variety of RNA samples in order to capture all possible transcripts expressed in these ES cells. Raw microarray data were normalized using the SNNLERM algorithm,²¹ and differentially expressed genes were determined using ANOVA considering three biological replicates. Hierarchical clustering, and the Self-Organizing Tree Algorithm (SOTA) were used to cluster groups of genes judged as statistically significant by ANOVA analysis, and such analyses as well as Gene Ontology (GO) analysis were implemented using tools of the MultiExperiment Viewer (MeV) (The Institute for Genomic Research [http://www.tigr.org/software/tm4/menu/TM4_Biotechniques_2003.pdf]).

Metabolic measurements and carbon balances

Each day over a period of 8 h, four culture-supernatant samples were taken from the cultures and flash-frozen. Samples were thawed just prior to analysis. Glucose, lactate, glutamine, and glutamate were measured using the YSI 2700 SELECT biochemistry analyzer (YSI, Ohio) according to the manufacturer's instructions, using four membranes to detect the four metabolites in one reading. The readings corresponding to each metabolite or glucose concentration (expressed as mmol/L) were averaged from three biological replicate experiments. Fluxes were expressed as $\text{mmol} \times \text{hr}^{-1} \times (\text{g-cell dry weight})^{-1}$. The total amount of each compound was calculated based on the total volume present in the culture at the time of sampling and the volume of the sample. Cell numbers were converted in g-cell dry weight using an average dry weight of 230 pg dry weight per cell. Carbon balance calculations were performed as detailed by Stephanopoulos et al.²² Briefly, molecular masses of all molecules considered in the production of biomass were normalized by their number of carbon atoms. For each carbon-containing species, the volumetric flux ($\text{g} \times \text{L}^{-1} \times \text{hr}^{-1}$) was calculated. Then, the flux of carbon atoms was calculated as $(\text{volumetric flux})/(\text{molecular mass expressed in carbon atom molecular mass})$. Finally, the balance closing is the % difference between the sum of all the species that are transformed and all the species that are produced. An example of calculation can be found in Supporting Information. Table 1 shows the closing for carbon balance. More than half of the measurements closed with an error below 15%, and only five sets of measurements had closings which were above 20%, four in the EB cultures and one in the Gelatin cultures. A 20% error in the closing of carbon balances was considered acceptable²³ because the model only considered prime variables.

Table 1. Carbon Balance Closing

Day	Embryoid Body	Gelatin	Matrigel
1	19.2%	21.6%	18.7%
2	6.4%	6.9%	7.3%
3	24.1%	6.6%	3.7%
4	20.1%	2.5%	1.8%
5	41.4%	19.0%	6.2%
6	21.0%	11.1%	6.6%
7	15.6%	12.6%	1.3%

Carbon-balance closings for each day and culture condition. The carbon-balance closing is the % difference between the sum of all the species that are transformed and all the species that are produced as detailed in Methods.

Metabolic flux analysis

Based on the total number of directly measured compounds and the degrees of freedom available, 15 stoichiometric metabolic reactions from the central metabolic pathway and eight transport steps were considered for the construction of a metabolic model. Briefly, the system consists of 35 compounds, of which 10 (ATP, P, ADP, NAD, NADH, Acetyl CoA, CoA, FAD, FADH, SuccinylCoA) are present in five conserved moieties, representing quantities that are conserved in a system, regardless of the individual reaction rates, i.e., these five conserved moieties define five singularities in the stoichiometric matrix. The system has three degrees of freedom [N^0 of base vectors of the null space of the stoichiometric matrix (3)] and the directly measured metabolites considered in the analysis were 3 (glucose, lactate, and glutamine; glutamate was used as internal control), making the model a determined system. MFA was based on these reactions. The software InSilico (Insilico Biotechnology AG, Stuttgart University) was used to implement the model and perform the corresponding calculations. Prior to MFA analysis, fluxes were normalized by the flux of glucose entering the cell, i.e., each flux was divided by the glucose flux for that particular set of data. This normalization allows easy comparison among different time points and conditions. The values of the fluxes resulting from the MFA will have a negative value if the flux maintains the direction of the canonical reaction (i.e. the usual direction considered for that flux). On the contrary, if the flux has a positive value, the calculated flux is in the opposite direction.

Metabolic Reactions Considered:

1. Biomass Synthesis:
 $0.000383309 \text{ *cysteine} + 0.020772276 \text{ *glucose} + 0.037695247 \text{ *glutamine} + 0.000591041 \text{ *glutamate} \Rightarrow \text{biomass}$
2. Glucose \Rightarrow Pyruvate:
 $\text{Glucose} + 2 \text{ *ADP} + 2 \text{ *NAD} + 2 \text{ *P} \Rightarrow 2 \text{ *H} + 2 \text{ *ATP} + 2 \text{ *NADH} + 2 \text{ *Pyruvate} + 2 \text{ *H}_2\text{O}$
3. Malate \Leftrightarrow Oxaloacetic Acid:
 $\text{Malate} + \text{NAD} \Leftrightarrow \text{Oxaloacetic Acid} + \text{NADH} + \text{H}$
4. Pyruvate \Leftrightarrow Acetyl CoA:
 $\text{Pyruvate} + \text{NAD} \text{ *CoA} \Leftrightarrow \text{Acetyl CoA} + \text{CO}_2 + \text{NADH}$
5. Oxaloacetic Acid \Leftrightarrow α -ketoglutarate:
 $\text{Acetyl CoA} + \text{Oxaloacetic Acid} + \text{H}_2\text{O} + \text{NAD} \Leftrightarrow \text{CO}_2 + \alpha\text{-ketoglutarate} + \text{NADH} + \text{CoA} + \text{H}$
6. α -ketoglutarate \Leftrightarrow SuccinylCoA:
 $\alpha\text{-ketoglutarate} + \text{CoA} + \text{NAD} + 2 \text{ *H} \Leftrightarrow \text{CO}_2 + \text{SuccinylCoA} + \text{NADH} + 2 \text{ *H}$
7. Fumarate \Leftrightarrow Malate:
 $\text{Fumarate} + \text{H}_2\text{O} \Leftrightarrow \text{Malate}$

8. Malate \Leftrightarrow Pyruvate:
 $\text{Malate} + \text{NAD} \Leftrightarrow \text{CO}_2 + \text{Pyruvate} + \text{NADH}$
9. Pyruvate \Leftrightarrow Lactate:
 $\text{Pyruvate} + \text{NADH} + 2 \text{ *H} \Leftrightarrow \text{Lactate} + \text{NAD}$
10. Glutamine \Leftrightarrow Glutamate:
 $\text{Glutamine} + \text{ADP} + \text{P} \Leftrightarrow \text{Glutamate} + \text{NH}_3 + \text{ATP}$
11. Glutamate \Leftrightarrow α -ketoglutarate:
 $2 \text{ *Glutamate} + \text{NAD} \Leftrightarrow \alpha\text{-ketoglutarate} + \text{glutamine} + \text{NADH} + \text{H}$
12. SuccinylCoA \Leftrightarrow Succinate:
 $\text{SuccinylCoA} + \text{ADP} + \text{P} \Leftrightarrow \text{Succinate} + \text{ATP} + \text{CoA}$
13. Succinate \Leftrightarrow Fumarate:
 $\text{Succinate} + \text{FAD} \Leftrightarrow \text{Fumarate} + \text{FADH}_2$
14. Oxidative phosphorylation I:
 $\text{NADH oxidation: } 2 \text{ *NADH} + 4 \text{ *H} + \text{O}_2 + 2 \text{ *ADP} + 2 \text{ *P} \Rightarrow 2 \text{ *NAD} + 4 \text{ *H}_2\text{O} + 2 \text{ *ATP}$
15. Oxidative Phosphorylation II:
 $\text{FADH}_2 \text{ oxidation: } 2 \text{ *FADH}_2 + \text{O}_2 + 2 \text{ *ADP} + 2 \text{ *P} + 2 \text{ *H} \Leftrightarrow 2 \text{ *FAD} + 2 \text{ *ATP} + 4 \text{ *H}_2\text{O}$

Transport Reactions (Steps) Considered:

1. Glucose transport:
 $\text{glucose}_{\text{Cytoplasm}} = \text{glucose}_{\text{external}}$
2. Oxygen transport:
 $\text{O}_2_{\text{Cytoplasm}} = \text{O}_2_{\text{external}}$
3. Carbon Dioxide transport:
 $\text{CO}_2_{\text{Cytoplasm}} = \text{CO}_2_{\text{external}}$
4. Glutamine transport:
 $\text{Glutamine}_{\text{Cytoplasm}} = \text{glutamine}_{\text{external}}$
5. Proton transport:
 $\text{H}^+_{\text{Cytoplasm}} = \text{H}^+_{\text{external}}$
6. H₂O transport:
 $\text{H}_2\text{O}_{\text{Cytoplasm}} = \text{H}_2\text{O}_{\text{external}}$
7. NH₃ transport:
 $\text{NH}_3_{\text{Cytoplasm}} = \text{NH}_3_{\text{external}}$
8. Lactate transport:
 $\text{Lactate}_{\text{Cytoplasm}} = \text{Lactate}_{\text{external}}$

Statistical Analysis and Error Propagation Supporting Information spreadsheet contains the primary data of the experimentally determined average fluxes and associated errors. We also include a “sensitivity matrix” based on our model, which shows the error associated with the calculated flux, based on the error associated with the experimentally measured flux. For example, a number of 0.5 for rate Glucose-to-pyruvate associated to the experimentally measured glucose flux means that if the experimentally measured glucose flux has a 1% associated error, the error associated with the calculated rate glucose-to-pyruvate 0.5%.

In general terms, the errors associated to the measured fluxes are never higher than 5%. The sensitivity matrix values are usually below 1, with the exception of water transport, ammonia transport, and biomass synthesis. Therefore, the associated errors with the calculated fluxes are below 5%.

Results and Discussion

Metabolic flux analysis vs. microarray-based gene-expression analysis

Figure 1 (and Supporting Information slide) represents the central metabolic pathways considered in the construction of the MFA model, which consist of 15 metabolic fluxes and eight transport reactions (steps). For each metabolic reaction, calculated fluxes are depicted in plots, while the heat maps

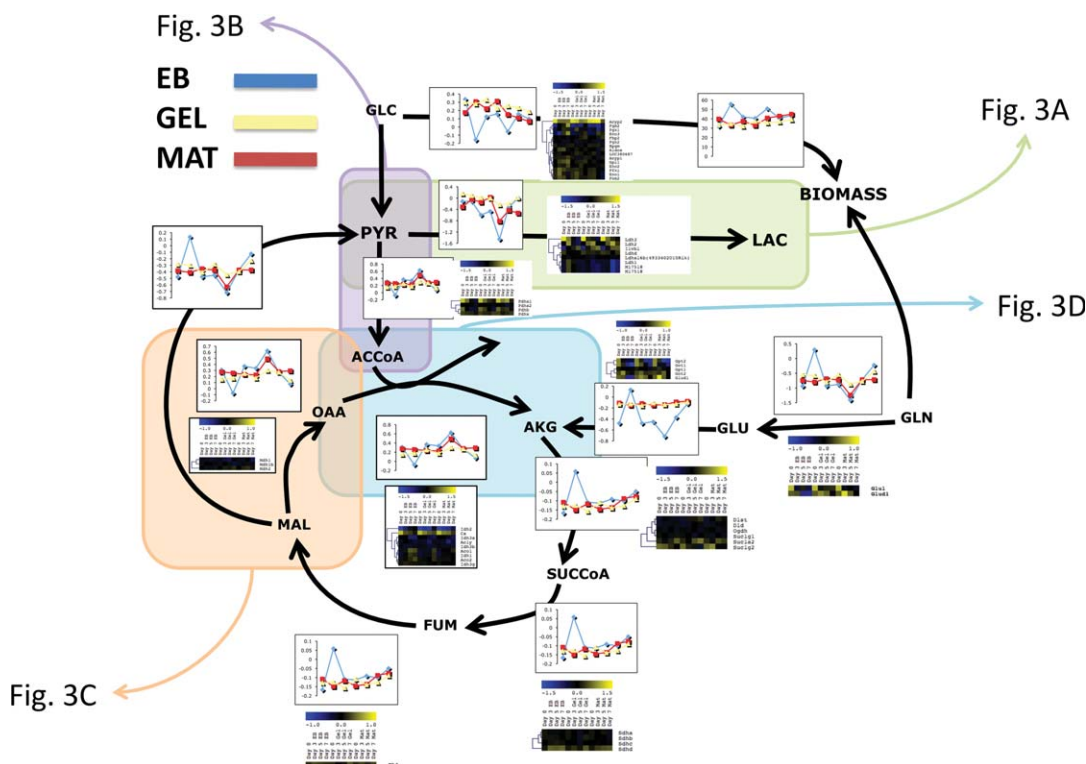


Figure 1. Central Metabolic Pathways of mouse ES cells.

Plots represent the calculated flux for each particular pathway (EB in blue, GEL in yellow and MAT in red). Fluxes were calculated for each day between Days 1 to 7. Heat maps represent the gene expression level for genes involved in each particular step.

correspond to the expression ratios (from the microarray analysis) for genes involved in that reaction (or lumped reactions). Detailed flux values calculated for all conditions (EB, GEL, and MAT) and days are shown in Supporting Information Tables 1, 2, and 3. Figure 1 (and Supporting Information slide) allows for a quick comparison between the calculated metabolic-flux values and the gene-expression data of genes involved in a particular set of metabolic reactions for each culture/differentiation condition and day. Thus, it is possible to easily identify interesting qualitative relations, which can be subsequently analyzed in more depth.

The flux for biomass production is temporally largely invariant for all three differentiation conditions, but other core fluxes show large temporal changes in the EB but not in the GEL or MAT conditions

Figures 2A–C (and Supporting Information Tables 1, 2, and 3) plot a set of select calculated fluxes for EB, GEL, and MAT, respectively. The data show that the flux toward biomass is relatively invariant compared to most other fluxes: the variation of biomass flux is around 40%, 25%, and 18% for EB, GEL, and MAT, respectively. In contrast, variations in other fluxes are over 60% for the GEL and MAT conditions, and up to 500% in EB (the only exception is the flux for the (minor) oxidative phosphorylation II reaction of $FADH_2$ oxidation). These results show that, while the biomass production, as assessed by metabolic-flux analysis, is maintained with a maximum temporal variation of 40%, most other analyzed metabolic fluxes display a much larger temporal variation (up to 500%) during ES-cell differentiation. This suggests a major redistribution of the fluxes in the central metabolism in a differentiation-protocol dependent manner. This temporal redistribution of fluxes correlates qualitatively with the changes in gene expression patterns as discussed below.

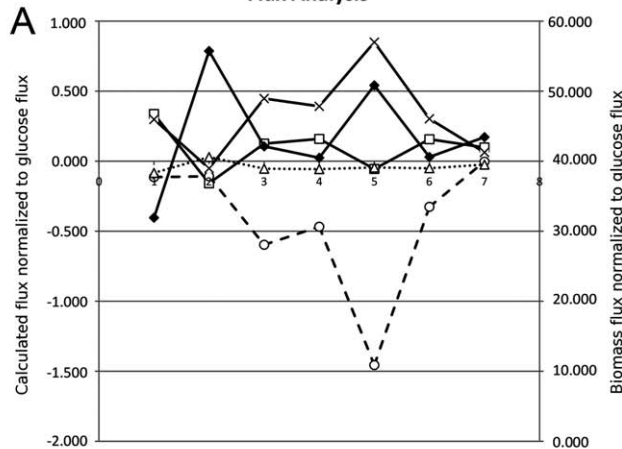
A major change in many metabolic fluxes occurs between Days 4 and 5. Specifically, the fluxes corresponding to the reactions: Malate \rightarrow Oxaloacetic Acid (Figure 3C), Pyruvate \rightarrow Acetyl CoA (Figure 3B) and Oxaloacetic Acid \rightarrow α -ketoglutarate (Figure 3D) increase by 100% for the EB and GEL conditions, but to a lower extent in the MAT condition. The other big change noticeable at Day 5 is the flux of the (major) oxidative phosphorylation reaction I (NADH oxidation); by 166% in EB, 100% in GEL, and 200% in MAT. Examination of the gene expression ratios shows that for most genes the largest variation in gene expression occurs between Days 3 and 5 (no measurement at Day 4). Thus, both metabolic-flux and gene-expression analysis, point to an event between Days 3 and 5 that triggers major changes at both the metabolic and the gene expression level.

It is noteworthy that the fluxes of the oxidative-phosphorylation reactions associated with NADH oxidation are mirror images of the pyruvate-to-lactate fluxes, both of which involve NADH consumption.

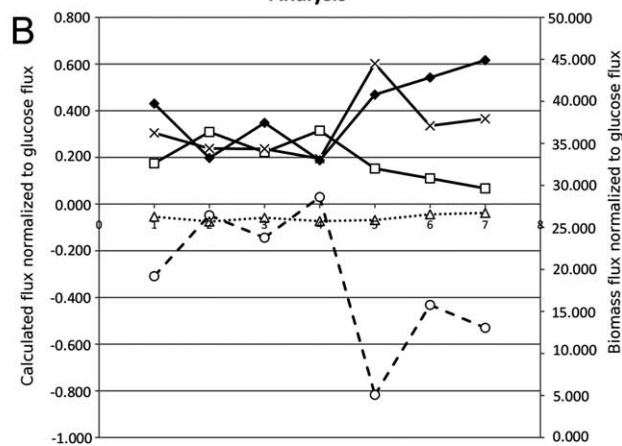
The pyruvate to lactate fluxes and the gene expression profiles of lactate dehydrogenase isoforms

Figure 3 shows a “close-up” of four key fluxes of Figure 1, namely pyruvate to lactate, pyruvate to acetyl-CoA, malate to oxaloacetate, and oxaloacetate to α -ketoglutarate. The flux from pyruvate to lactate (Figure 3A) displays a relatively invariant behavior for the GEL and MAT differentiation protocols but large temporal variations in the EB differentiation protocol. The corresponding gene-expression patterns for Ldh1, Ldh2 show a higher variation for the EB compared to the GEL and MAT conditions. Such metabolic and gene expression patterns could reveal information about the differentiated cell types (e.g., skeletal muscle or cardiac muscle) favored under different culture modalities and different times.

Calculated fluxes for Embryoid Body condition (EB) using Metabolic Flux Analysis



Calculated fluxes for Gelatin condition (GEL) using Metabolic Flux Analysis



Calculated fluxes for Matrigel condition (MAT) using Metabolic Flux Analysis

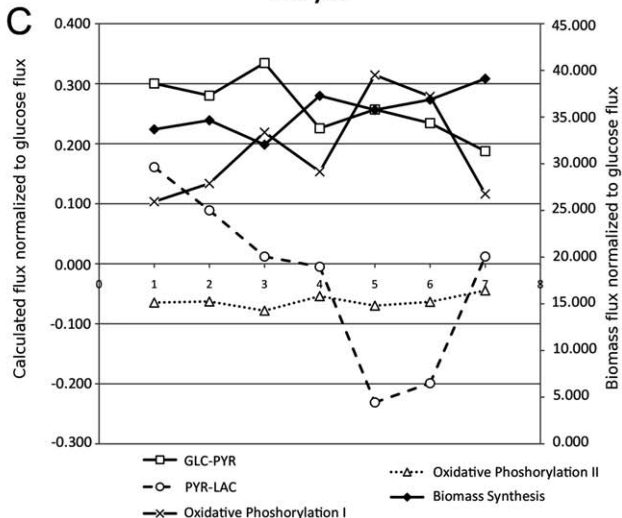


Figure 2. Calculated fluxes for A: Embryoid Body (EB), B: Gelatin (GEL), and C: Matrigel (MAT) conditions using Metabolic Flux Analysis.

Lactate fluxes show different patterns for each differentiation protocol. For the EB condition the flux is always in the direction of lactate formation (negative sign in every value,) with an increase in production from Day 1 to Day 5 and an abrupt decrease in Days 6 and 7. In the GEL condition, the

flux is almost zero from Day 1 to Day 4 with a sharp increase on Day 5. The lactate fluxes for MAT are the most invariant of the three conditions with mostly positive or small negative values. We conclude that lactate metabolism is dependent on the type of the differentiation protocol used, and in fact consistent with the predicted behavior based on oxygen availability in these differentiation protocols. As previously discussed,¹⁹ the EB cell aggregates derived from ES cells result in nutrient (and notably oxygen) and metabolite transport limitations from/to the core of the EB to/from the culture medium, especially during the first 5 days prior to vascularization²⁴ (note the change in the lactate flux pattern on Day 5; Figure 3A). Under such anoxic conditions, cells typically exhibit a strong lactogenic pattern as shown here for the EB conditions. This is in contrast to the surface-type GEL and MAT cultures, whereby cells are considerably better oxygenated.

The gene expression profiles for the enzymes responsible for the conversion of pyruvate to lactate are shown in Figures 4A–C. The figures show different gene expression profiles for the three genes encoding the enzyme isoforms, which form the heterotetrameric enzyme Lactate dehydrogenase, LDH. In particular, the profile of Ldh1 (Figure 4A), the monomer that is mainly present in skeletal muscle and produces lactate in anaerobic conditions, increases from Day 0 to Day 3 and afterward decreases for EB and GEL. In MAT, this profile is constant during the first 3 days of differentiation, and then decreases abruptly at Day 5. At Day 7 the expression ratio increases but to a lower level than the initial value. Another isoform, Ldh2 (Figure 4B), which is mainly present in cardiac muscle and which is inhibited by high pyruvate concentrations, shows a sharp increase from Day 0 to Day 3 and afterward a slow decrease (depending on the condition EB, GEL, or MAT). The Ldh3 isoform (Figure 4C), corresponding to the Ldh monomer that has been found specifically in male sperm, shows a sharp decrease during all differentiation conditions.

The lactate metabolic flux in EB correlates with the gene expression profile of Ldh1, which increases from Day 0 to Day 3 (Figure 2A) and then decreases and reaches a similar level to that found in the undifferentiated state (Day 0), and also shows higher levels compared to the other two conditions (GEL and MAT). Also worth noting is the gene expression profile of Ldh2 in the EB condition, which shows a sharp decrease from Day 3 to Day 5, and which could possibly be correlated with the higher flux from pyruvate to lactate from Day 4 to Day 5.

Lactate fluxes in the GEL condition correlate with constant expression levels of Ldh1 during the first 3 to 4 days. The increase of Ldh2 level on Day 5 could possibly explain the sharp decrease in the pyruvate to lactate flux observed in Days 5 to 7. Lactate fluxes in MAT correlate with the gene expression profile of Ldh1, which decreases from Day 0 to Day 5 and increases from Day 5 to 7; Ldh2 increases from Day 0 to Day 5 and decreases from Day 5 to Day 7.

Conclusions

We found that there is a qualitative correlation between the calculated fluxes based on direct metabolite measurements, and the gene expression profiles, obtained through microarray analysis. This correlation is more evident for differences in the flux for energy production, in particular, between differentiation conditions for reactions: pyruvate to

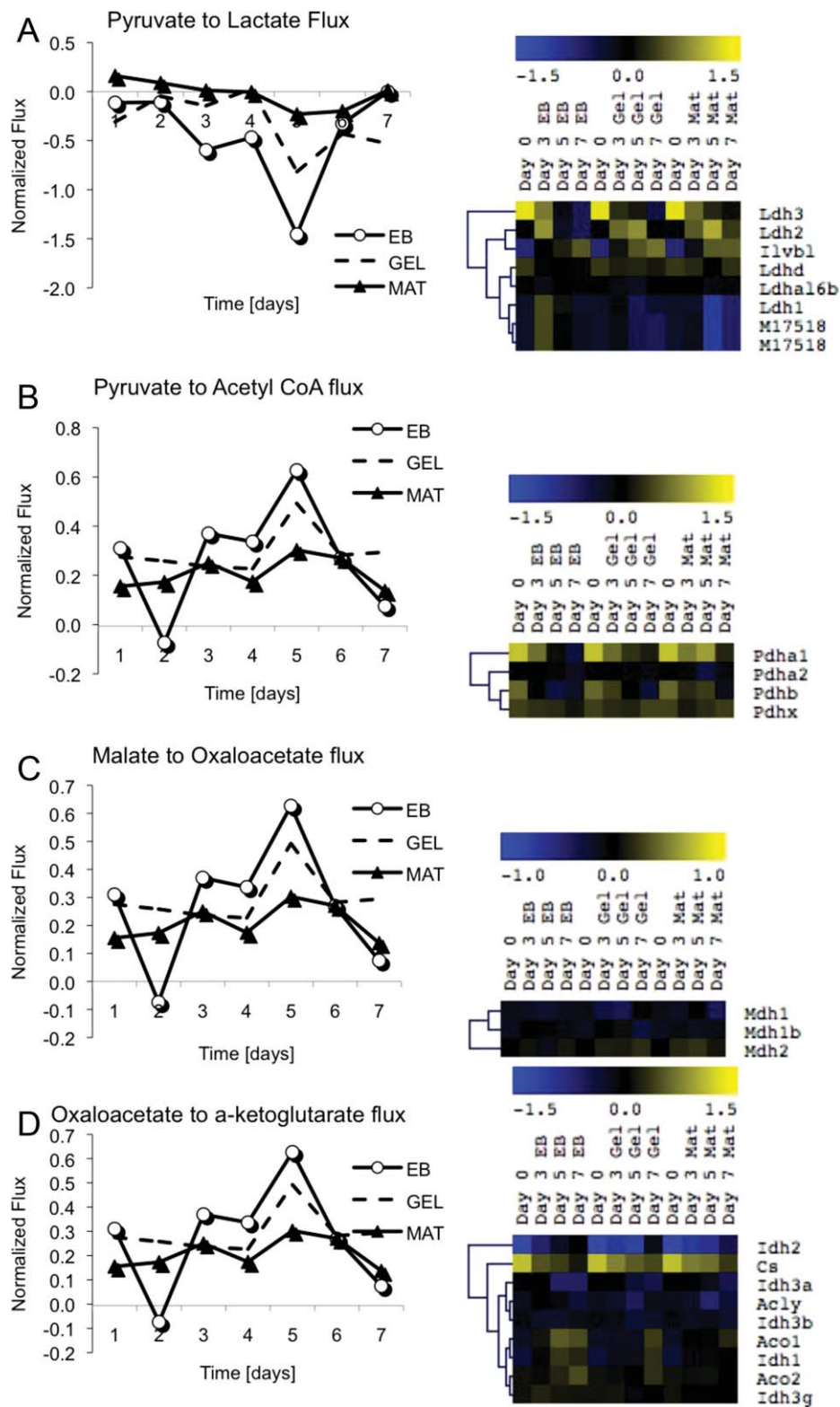


Figure 3. Metabolic fluxes calculated through MFA together with a heat map of gene expression for the genes involved in four key steps from Figure 1.

Fluxes were normalized to the incoming glucose flux for better comparison and calculated for a period of 7 days. Gene expression heat maps show the level of expression of genes compared to the control. **A:** Pyruvate to lactate; **B:** Pyruvate to Acetyl CoA; **C:** Malate to Oxaloacetate; **D:** Oxaloacetate to α -ketoglutarate.

lactate, malate to oxaloacetate pyruvate to acetylCoA, and oxaloacetate to α -ketoglutarate. These changes correlate qualitatively with changes in the gene expression profiles.

It is interesting to see that a qualitative jump in the values calculated for all metabolic fluxes observed across all condi-

tions in the time span between Days 4 and 5 is also reflected in the increase of the variation of the gene expression happening between Days 3 and 5 (Figures 1 and 3). This defines a key event in differentiation, which is triggered between Days 3 and 5, when considering the gene expression profiles

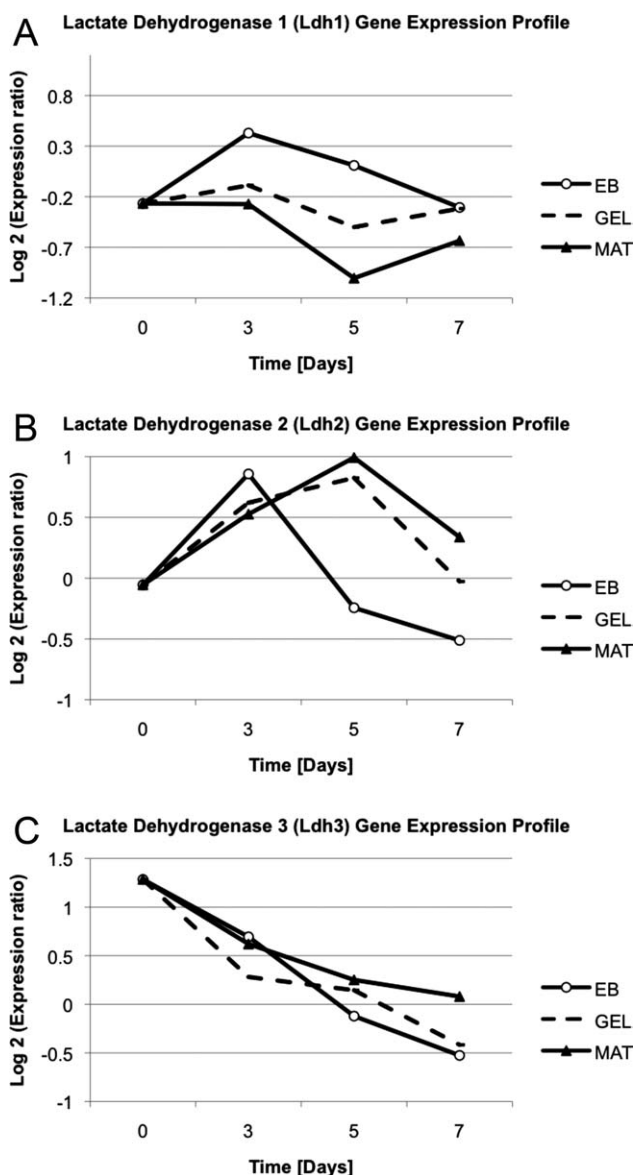


Figure 4. Temporal gene expression profile of lactate-dehydrogenase genes in the differentiation conditions EB, GEL, and MAT.

A: Lactate Dehydrogenase 1 (Ldh1) gene expression profile.
 B: Lactate Dehydrogenase 2 (Ldh2) gene expression profile.
 C: Lactate Dehydrogenase 3 (Ldh3) gene expression profile.

(no sample on Day 4), and more specifically from Day 4 to 5 when we consider the metabolic flux changes. This behavior has not been reported in the literature before.

In the limited studies that have been reported in the literature on prokaryotes (e.g., Ref. 15) or eukaryotes (e.g., Ref. 12), the correlation between fluxes and gene expression patterns varied from acceptable to none. Theoretical and experimental studies have examined fundamental issues as to why gene expression might correlate (or not) to protein-level expression,^{25,26} but the correlation to fluxes adds another level of complexity,^{27,28} which is unlikely to get resolved in the absence of detailed data on metabolites and enzyme-level regulation. This study shows a reasonably, qualitative correlation in the behavior of metabolic fluxes with gene expression patterns. It is possible that this correlation was observed due to the longer doubling time of differentiating ES cells, as opposed to yeast and bacteria or fast growing mammalian

cell lines, where the shorter doubling time would not allow the effects of gene expression changes to be reflected on metabolic-flux changes.

Acknowledgment

We acknowledge financial support from Millennium Scientific Initiative (MSI, Project ICM P05-001-F), a Fulbright Fellowship, NIH USA (Grant R01-GM065476), and FONDECYT project 1061119.

Literature Cited

1. Wobus AM, Boheler KR. Embryonic stem cells: prospects for developmental biology and cell therapy. *Physiol Rev.* 2005;85:635–678.
2. Doetschman TC, Eistetter H, Katz M, Schmidt W, Kemler R. The in vitro development of blastocyst-derived embryonic stem cell lines: formation of visceral yolk sac, blood islands and myocardium. *J Embryol Exp Morphol.* 1985;87:27–45.
3. Palacios R, Golunski E, Samaridis J. In vitro generation of hematopoietic stem cells from an embryonic stem cell line. *Proc Natl Acad Sci USA.* 1995;92:7530–7534.
4. Potocnik AJ, Nielsen PJ, Eichmann K. In vitro generation of lymphoid precursors from embryonic stem cells. *EMBO J.* 1994;13:5274–5283.
5. Goldring K, Partridge T, Watt D. Muscle stem cells. *J Pathol.* 2002;197:457–467.
6. Assady S, Maor G, Amit M, Itskovitz-Eldor J, Skorecki KL, Tzukerman M. Insulin production by human embryonic stem cells. *Diabetes.* 2001;50:1691–1697.
7. Wobus AM, Guan K, Yang HT, Boheler KR. Embryonic stem cells as a model to study cardiac, skeletal muscle, and vascular smooth muscle cell differentiation. *Methods Mol Biol.* 2002;185:127–156.
8. Correia AS, Anisimov SV, Li JY, Brundin P. Growth factors and feeder cells promote differentiation of human embryonic stem cells into dopaminergic neurons: a novel role for fibroblast growth factor-20. *Front Neurosci.* 2008;2:26–34.
9. Baetge EE. Production of beta-cells from human embryonic stem cells. *Diabetes Obes Metab.* 2008;10(Suppl 4):186–194.
10. Deshpande R, Yang TH, Heinzle E. Towards a metabolic and isotopic steady state in CHO batch cultures for reliable isotope-based metabolic profiling. *Biotechnol J.* 2009;4:247–263.
11. Dorka P, Fischer C, Budman H, Schärer JM. Metabolic flux-based modeling of mAb production during batch and fed-batch operations. *Bioprocess Biosyst Eng.* 2009;32:183–196.
12. Banta S, Vemula M, Yokoyama T, Jayaraman A, Berthiaume F, Yarmush ML. Contribution of gene expression to metabolic fluxes in hypermetabolic livers induced through burn injury and cecal ligation and puncture in rats. *Biotechnol Bioeng.* 2007;97:118–137.
13. Chan C, Berthiaume F, Lee K, Yarmush ML. Metabolic flux analysis of hepatocyte function in hormone- and amino acid-supplemented plasma. *Metab Eng.* 2003;5:1–15.
14. Yoo H, Antoniewicz MR, Stephanopoulos G, Kelleher, JK. Quantifying reductive carboxylation flux of glutamine to lipid in a brown adipocyte cell line. *J Biol Chem.* 2008;283:20621–20627.
15. Tummala SB, Junne SG, Paredes CJ, Papoutsakis ET. Transcriptional analysis of product-concentration driven changes in cellular programs of recombinant *Clostridium acetobutylicum* strains. *Biotechnol Bioeng.* 2003;84:842–854.
16. Fatumo S, Plaimas K, Mallm JP, Schramm G, Adebisi E, Oswald M, Eils R, König R. Estimating novel potential drug targets of *Plasmodium falciparum* by analysing the metabolic network of knock-out strains in silico. *Infect Genet Evol.* 2009;9:351–358.
17. Bonarius HP, Hatzimanikatis V, Meesters KP, de Gooijer CD, Schmid G, Tramper J. Metabolic flux analysis of hybridoma cells in different culture media using mass balances. *Biotechnol Bioeng.* 1996;50:299–318.

18. Bonarius HP, Ozemre A, Timmerarends B, Skrabal P, Tramper J, Schmid G, Heinzle E. Metabolic-flux analysis of continuously cultured hybridoma cells using $(^{13}\text{C})\text{CO}_2$ mass spectrometry in combination with (^{13}C) -lactate nuclear magnetic resonance spectroscopy and metabolite balancing. *Biotechnol Bioeng.* 2001;74:528–538.
19. Sepulveda DE, Andrews BA, Asenjo JA, Papoutsakis ET. Comparative transcriptional analysis of embryoid body versus two-dimensional differentiation of murine embryonic stem cells. *Tissue Eng Part A.* 2008;14:1603–1614.
20. Nagy A, Rossant J, Nagy R, Abramow-Newerly W, Roder JC. Derivation of completely cell culture-derived mice from early-passage embryonic stem cells. *Proc Natl Acad Sci USA.* 1993;90:8424–8428.
21. Yang H, Haddad H, Tomas C, Alsaker K, Papoutsakis ET. A segmental nearest neighbor normalization and gene identification method gives superior results for DNA-array analysis. *Proc Natl Acad Sci USA.* 2003;100:1122–1127.
22. Stephanopoulos GN, Aristidou AA, Nielsen J. *Metabolic Engineering: Principles and Methodologies.* Academic Press: San Diego, California; 1998:119–121.
23. Goudar CT, Biener R, Konstantinov KB, Piret JM. Error propagation from prime variables into specific rates and metabolic fluxes for mammalian cells in perfusion culture. *Biotechnol Prog.* 2009;25:986–998.
24. Wartenberg M, Donmez F, Ling FC, Acker H, Hescheler J, Sauer H. Tumor-induced angiogenesis studied in confrontation cultures of multicellular tumor spheroids and embryoid bodies grown from pluripotent embryonic stem cells. *FASEB J.* 2001;15:995–1005.
25. Lee PS, Shaw LB, Choe LH, Mehra A, Hatzimanikatis V, Lee KH. Insights into the relation between mRNA and protein expression patterns. II. Experimental observations in *Escherichia coli.* *Biotechnol Bioeng.* 2003;84:834–841.
26. Mehra A, Lee KH, Hatzimanikatis V. Insights into the relation between mRNA and protein expression patterns. I. Theoretical considerations. *Biotechnol Bioeng.* 2003;84:822–833.
27. Thomas R, Paredes CJ, Mehrotra S, Hatzimanikatis V, Papoutsakis ET. A model-based optimization framework for the inference of regulatory interactions using time-course DNA microarray expression data. *BMC Bioinformatics.* 2007;8:12.
28. Thomas R, Mehrotra S, Papoutsakis ET, Hatzimanikatis V. A model-based optimization framework for the inference on gene regulatory networks from DNA array data. *Bioinformatics* 2004;20:3221–3235.

Manuscript received Sept. 15, 2009, and revision received Feb. 13, 2010.